New on-orbit calibration approach of SNPP VIIRS reflective solar bands using the full profile of direct solar illumination of solar diffuser

Junqiang Sun, Mike Chu, and Menghua Wang

***Abstract*—A methodological variant of the standard on-orbit calibration of reflective solar bands (RSBs) is presented for the Visible Imaging Infrared Radiometer Suite (VIIRS) housed in the Suomi National Polar-orbiting Partnership (SNPP) satellite. The new variant uses the full profile of direct solar illumination of the solar diffuser (SD), including both full and partial illuminations, to characterize the on-orbit gain change of the RSBs, differing from the standard approach that uses a smaller "sweet spot" sub-interval within the full-illumination stage. The extended incident angular range of the solar light requires a new characterization analysis of the impact of the transmission function of the SD screen, SD bidirectional reflectance factor (BRF) and other affected calibration steps. Instead of the standard a priori derivation of the known characterization functions for the wider range, this analysis directly characterizes their manifested impact in the instrument data through a step-by-step extraction from a selected three-year period to build up a series of intermediate functions that are applicable mission-long. This newly adopted procedure presents a significant simplification as well as more clarity of the characterization analysis. The new RSB calibration coefficient of the full-profile approach is extracted for all 14 RSBs of SNPP VIIRS and is shown to be stable and smooth at the level of 0.1%. For bands M5 and above, the full-profile result achieves excellent agreement with the standard result, whereas results for bands M1−M4 diverge, in particular up to 2% for band M1, the shortest wavelength RSB at 410 nm. The finding elucidates a key challenge of the on-orbit RSB calibration arising from the non-trivial angular dependence of the on-orbit degradation of SD that introduces calibration error into any SD-based approach, such that the on-orbit RSB calibration result is not stable with different choices of the angular range of incident and outgoing light with respect to the SD. A detailed discussion of the non-trivial angular dependence in SD degradation is provided in the context of the known on-orbit RSB calibration results and recent findings, including discrepancy with the lunar-based calibration for bands M1−M4.**

***Index Terms*—Calibration, Radiometry, Remote Sensing**

I. Introduction

The coming generations of Earth sciences and climate studies will see further explosions of sensor data with more high-performing multispectral sensors being launched into operations. Following the success of the twin units of MODerate-resolution Imaging Spectroradiometer (MODIS) in the Terra and Aqua spacecrafts, launched on 18 December 1999 and 4 May 2002 [1,2], respectively, and the Visible Infrared Imaging Radiometer Suite (VIIRS) in the Suomi National Polar-orbiting Partnership (SNPP) satellite launched on 28 October 2011 [3], more follow-on sensors adopting similar designs and operations have either recently launched or are in planning, in particular adopting a nearly identical on-orbit calibration strategy. For example, the Sentinel-3 mission, launched on 26 February 2016, houses the 22-band Ocean and Land Colour Instrument (OLCI) and the companion instrument Sea and Land Surface Temperature Radiometer (SLSTR) [4]. The NOAA-20 VIIRS, the first of the four follow-on VIIRS in the Joint Polar Satellite System (JPSS) series formerly known as JPSS-1 (J1) VIIRS, was launched on 18 November 2017.

These current and next-generation multispectral sensors adopt a very similar on-orbit calibration methodology using a full suite of on-board calibrators (OBCs) to carry out regular on-orbit calibration measurements of the performance of the detectors throughout the aging of the sensor. Their spectral bands are either reflective solar bands (RSBs) or thermal emissive bands (TEBs), which follow different calibration strategies. For the RSBs, the use of a diffuser panel with nearly ideal reflectance property, commonly referred to as the solar diffuser (SD), is at the core of the on-orbit calibration strategy [5]. The fundamental premise of the SD-based RSB calibration operation is that the radiance, using solar exposure as the illumination source, reflecting off SD is quantifiable, thus providing a reliable calibration reference upon which the

This paper is submitted on March 3, 2018. This work was supported by the Joint Polar Satellite System (JPSS) funding.

J. Sun is with Global Science and Technology, 7855 Walker Drive, Suite 200, Greenbelt, MD 20770 USA (e-mail: junqiang.sun@ noaa.gov).

M. Chu is with Cooperative Institute for Research in the Atmosphere, Colorado State University, Fort Collins, CO 80521 USA (mike.chu@noaa.gov).

M. Wang is with NOAA National Environmental Satellite, Data, and Information Service Center for Satellite Applications and Research E/RA3, 5830 University Research Ct., College Park, MD 20740, USA (e-mail: menghua.wang@noaa.gov).

performance of RSB can be analyzed. This approach has been utilized for MODIS and SNPP VIIRS [6-8]. Since the reflectance of SD also degrades on-orbit, an accompanying solar diffuser stability monitor (SDSM) makes regular scheduled measurements of degradation of SD [6−9].

This paper presents a new variant to the standard operational on-orbit RSB calibration methodology. While the operational procedure uses a small four-degree angular range called the "sweet spot" within the full-illumination interval of the SD, the new variant uses the entire illuminated interval, both partial and full, in the analysis of the RSB calibration coefficients, or F-factors. The new consideration to use the full-profile of direct solar illumination and the insights gained from it can potentially help to improve the current methodology or operational procedure. An entirely new empirical characterization procedure is shown to be simpler and cleaner; for example, it does not need to use the (two-dimensional) vignetting function (VF) for the effect of the solar intensity attenuation screen in front of the SD port and the bidirectional reflectance factors (BRFs) of the SD. This analysis directly extracts the impact of the manifested effects in the routine SD data via an examination of a three-year period for their removal. The overall result presented here is to be compared with Sun and Wang [8] on the standard RSB calibration of SNPP VIIRS.

An additional issue is to be addressed by the new result. It is well known that the RSB calibration for both MODIS and SNPP VIIRS has demonstrated long-term calibration inadequacies in both MODIS [10,11] and SNPP VIIRS [12]. For MODIS, the inadequate performance of the standard RSB calibration result for the shortest wavelength bands, such as in MODIS bands 3, 8, and 9, motivated the Collection 6 methodology [10,11] that abandons the standard SD-based approach in favor of an Earth target-based analysis. For SNPP VIIRS, inconsistencies in the calibration result, such as disagreement with the lunar-based calibration analysis [12], are also evident. A series of independent investigations carried out by Sun and Wang [8,9,12,13] for SNPP VIIRS have led to significantly more accurate calibrated sensor radiance with 0.2% stability. One key finding among the results is the discovery of the "SD degradation non-uniformity (SDDNU) effect" [8,9,12,13,14], or the non-ideal anisotropic dependence in the degradation of the SD, shown to contribute long-term, systematic, and worsening error into the calibration result of SNPP VIIRS that is particularly significant for bands M1–M4. The mitigation of the drifting error is made through a "hybrid-method" [12] that resorts to the lunar-based analysis to set the long-term calibration baseline. A dedicated follow-up study examining the mission-long calibration data of RSB and SDSM proves the existence of the SDDNU effect [14] in both MODIS and SNPP VIIRS, thus confirms also a primary source of calibration bias that plagued MODIS RSB calibration. The source of the calibration error stems from the fact that the degradation of the SD as measured by the SDSM is the SD degradation~~specifically~~ in the outgoing direction toward the SDSM with respect to the SD normal and that SD degradation is outgoing direction dependent~~the angular dependence in SD degradation renders it incorrect~~. In principle, the SD degradation required for RSB calibration is in an entirely different outgoing angular direction – from the SD toward the RSBs in MODIS, or from the SD toward the Rotating Telescope Assembly (RTA), which directs light to the RSBs, in SNPP VIIRS. The standard methodology makes no distinction between the two different outgoing directions and assumes the SDSM-measured SD degradation as a valid substitute. The existence of SDDNU effect makes discrepant the two SD degradations at the two different outgoing angles, giving rise to worsening calibration bias as the effect accumulates over time. A more generalized statement is that the bidirectional reflectance distribution function (BRDF) of the SD changes its functional dependence on both the incoming and the outgoing angle with respect to the SD normal as the overall reflectance performance of SD degrades [14], as supported by optical reciprocity. The full profile result provides another demonstration that different incident angles to the SD leads to different calibration outcomes. The non-trivial and changing angular dependence in the BRDF of the SD therefore is a challenge for any SD-based formalism.

Despite the aforementioned challenge with the current standard SD-based calibration approach, the coming era of newer multispectral sensors firmly remains reliant on the use of the SD for on-orbit RSB calibration. Different considerations to the SD-based formalism can be highly beneficial. The new full-profile result is fully expected to generate a set of mission-long F-factor that diverges from the standard result, in particular for bands M1−M4, because of the SDDNU effect; however, the mitigation of the SDDNU effect [12] to restore calibration accuracy remains an separate issue outside the scope of any SD-based calibration.

The outline of this paper is as follows. Section 2 describes the illumination of SD and its use in both the standard operational procedure and the full-profile approach. Section 3 lays out the formalism and the data analysis procedure leading to the extraction of the full-profile F-factor. Section 4 presents the result and compare with the standard result. Section 5 summarizes and concludes.

II. CALIBRATION ALGORITHM OF THE FULL-PROFILE APPROACH

The algorithm of the full-profile approach preserves the standard calibration pipeline component-wise. A schematic of SNPP VIIRS on-board calibrator components is shown in Fig. 1. However, the extension of the angular range of light incident on the SD to include all direct solar illumination changes numerous characterizing steps and inputs. First and foremost, the larger angular range requires a reconsideration of all optical effects associated with the solar illumination. For example, the transmission function of the pin-holed attenuation screen placed in front of the SD port, the VF, that characterizes the vignetting effect of the screen pinholes, needs to be re-characterized to account for the larger angular range of the full-profile approach given that the originally derived standard VF for covers only a smaller angular range around the "sweet spot" [15,16]. In practice, the VF is not independently characterized, but together

with the BRF of the SD. This product of the BRF and VF [15], the BRF-VF product (BVP), is a critical input of the on-orbit RSB calibration. Since the vignetting effect itself, or the BVP function, and any residual of the characterization of the effect, necessarily follows a yearly cycle in accordance with the yearly orbital position around the Sun, the step-by-step extraction procedure herein directly examines the yearly pattern for an empirical characterization of the manifested effect. This is an independently new analysis that improves the quality of the derived result by averting the complicated a priori derivation of the various functions mentioned above. The derivation of the new BVP for the full-profile approach is not trivial given the greater complexity and the wider range involving also the partial illumination; this analysis instead uses the available instrument data, specifically via an examination of a selected three-year interval, to perform a straightforward extraction of the yearly patterns. The characterization functions of the yearly patterns, corresponding to the combined manifested effects of the various calibration components and the associated optical effects, can be directly and straightforwardly applied to mission-long data and for future RSB calibration work using the full-profile approach.

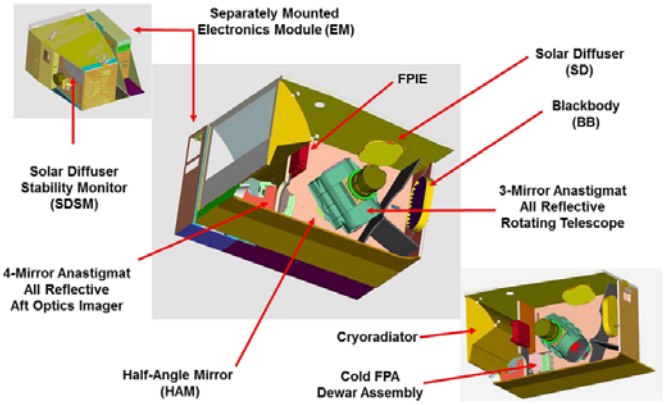

Fig. 1. SNPP VIIRS and the on-board calibrators.

A. *SD Observation*

Figure 2 shows the various solar angles in the instrument coordinate frame for SNPP VIIRS. For clarity and consistency with previous work [8,9,14], solar declination is primarily used in this analysis.

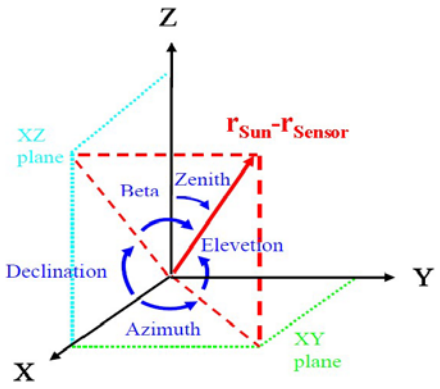

Fig. 2. Solar angles in the instrument coordinate system.

Figure 3 illustrates an example of the illumination of the SD in actual detector digital number (dn) with respect to solar declination angle through the daytime part of the orbit for Band M1 Detector 1 in high-gain stage. The illumination of the SD starts with the satellite approaching the terminator from the nightside, corresponding Fig. 3 the most-right side where declination is positive. As the satellite continues to move through its orbit, the declination angle decreases with time and becomes negative after the satellite crosses the terminator. When the SD port and the SD begin align with the sun direction, partial illumination starts and continues to rise until reaching full illumination due to direct alignment to the sun direction, shown in Fig. 3 as the plateau region in the middle of the peak. When the SD port and the SD move away from alignment with the sun direction, the illumination again drops to partial until finally loosing all direct solar exposure. The illumination of the SD, however, does not completely vanish throughout the daytime part of the orbit. It can be seen in Fig. 3 that SD continues to receive some weak signals two orders of magnitude lower. This low illumination comes from light scattered of Earth's surface that passes through the nadir-port. A parallel investigation on the use of the Earth-scattered light for RSB performance characterization also has been conducted [17]. The Earth-scatter light illumination actually impacts the full-profile approach analysis by blending some signals into the full profile of direct solar illumination. Where Earth-scattered light blends in its signals is shown in Fig. 3 by the small interval of 8° range between 0° declination and the green dashed vertical line at the left foot of the peak.

Figure 4 illustrates the direct solar illumination interval corresponding to the large peak in Fig. 3. The three stages of the solar illumination are the rising partial illumination from the right, the plateau in the middle due to full solar illumination that also changes with the angle, and the decreasing partial illumination on the left. This combined three-stage direct solar illumination is the subject of this analysis. The 4° sub-interval within the full illumination plateau, bounded by the two cyan dashed vertical lines between the solar declination angular range of 13° to 17°, is the "sweet spot" interval from which the measured data are used by the standard procedure to compute the calibration coefficient, or F-factor [9]. The region of the

weak signals at the green vertical dashed line at -7° also exhibits a smoother transitional behavior, and this weak signal turns out to have a small but noticeable effect on the new F-factor.

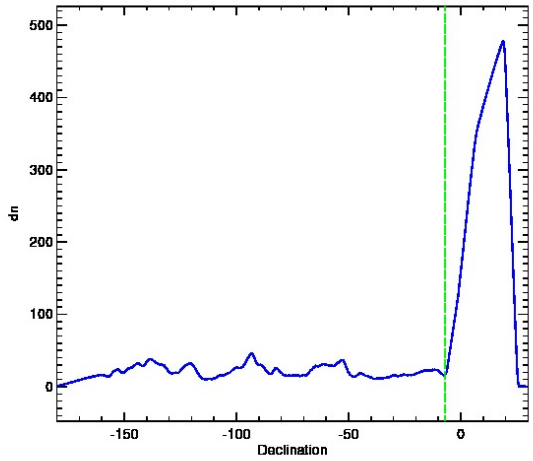

Fig. 3. SNPP VIIRS Band M1 Detector 1 high gain SD view response for the daytime portion of the orbit.

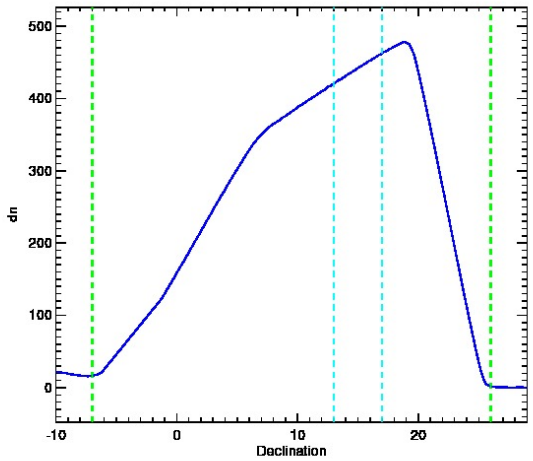

Fig. 4. The sweet spot for SNPP VIIRS Band M1 Detector 1 high gain stage is shown between the two vertical cyan dashed lines within the full illumination of the SD. The two vertical green dashed lines bound the full-profile of the direct solar illumination.

This methodological extension demonstrates the use the entire profile of the solar illumination of the SD, including both the full and the partial illumination as shown in Fig. 4, for the on-orbit calibration of RSBs. The extension of the illumination range does require, for example, an update of the BVP to cover the full angular range of direct solar illumination. However, this analysis does not attempt to derive the extended BVP nor go through the standard characterization for all components, but instead examines the actual trend of the band response for a direct characterization of the manifested effects. There are two clear advantages to this empirical characterization of the effects in the three-year data over the a priori derivation of the characterization functions specific to each calibration components and effects. The first is that the real impact of the overall combined optical effects may be more complex than the idealized behavior of each component, but the empirical characterization is neither dependent on the accuracy of the theoretical description nor concerned with the any specific technical details. The empirical approach simply captures all effects in entirety without needing to consider each effect individually. One specific detail to note is that BVP is a two-dimensional function requiring two solar angles, such as azimuth and declination, and the a priori derivation to characterize the optical effect is not trivial. But the analysis approach adopted here, by summing over the full-profile data as to be described later, provides an important simplification by effectively integrating away the dependence on the solar declination angle, leaving only the azimuth angle-dependent variation in the data to be characterized. The second is that the empirical characterization simultaneously leads to the F-factor of the full-profile approach since the manifested effects can be directly removed.

B. The Formalism

The radiance $L_{SD}(\lambda)$ from the SD as observed by the RSB for direct solar illumination at a given wavelength λ can be generalized for the full-profile approach as:

$$L_{SD}(\lambda,\beta,\phi) = I_{Sun}(\lambda)\cdot\cos(\theta_{SD})\cdot h(\lambda)\cdot\rho_{SD,RTA}(\lambda)\cdot\tau_{SDS}\cdot C_{Geo}/d_{ES}^2, \quad (1)$$

where $I_{Sun}(\lambda)$ is the solar irradiance per unit area on surface normal to the incident light at the distance of one Astronomical Unit (AU), β is the solar beta angle, ϕ is solar declination angle, θ_{SD} is the solar-zenith angle of the incident light to the SD, $h(\lambda)$ is the SD degradation (or H-factor) measured by the SDSM, $\rho_{SD,RTA}(\lambda)$ is the BRF of the SD in the direction toward the RTA which directs the light to the RSB, τ_{SDS} is the transmission function, or the VF, of the attenuation screen in front of the SD port, C_{Geo} is the characterizing function for other optical effects associated with the partial illumination within the full-profile, and d_{ES} is the Earth-Sun distance in AU at the time of measurement. This work elects to use solar beta angle β instead of solar azimuth angle in the description for convenience, although the two angles are not linearly independent and it is legitimate to use either angle. The product $\rho_{SD,RTA}(\lambda)*\tau_{SDS}$ in Eqn. (1) is the two-dimensional BVP function, as mentioned previously, that depends on the two solar angles β and ϕ. The characterizing function C_{Geo} accounts for the impact of the different viewing geometry and the optical effect associated with partial illuminations. Within the full-illumination interval including the sweet-spot, in principles, all geometric and optical effects are described by the BVP function, and therefore C_{Geo} is a constant of 1 during full-illumination. However, as the BVP function in the standard approach considers only the full and direct solar illumination as the typical condition, the formalism for the full-profile approach to include partial illuminations requires C_{Geo} as a compensating function to complete the description. In addition, other effects not yet considered can exist, and C_{Geo} can be viewed in greater generality as a master description including all additional effects. The result of this

analysis thus also tests the scope of the C_{Geo} function. If truly a geometric consideration due to partial illumination, then the C_{Geo} function should be fully captured by a characterization step solely basing on solar beta angle, and this result is to be shown and discussed later.

The data analysis for this work adopts a summation scheme of the instrument *dn* in the full-profile interval, equivalent to integrating illumination over solar declination within each event, to build up the mission-long data. This reduction of dimensionality is an important step that provides a key simplification for this analysis. For clarity and convenience, a radiance function, K_B, for each band B of wavelength λ, adjusted for the relative spectral response (RSR) and integrated over the solar declination ϕ of the full-profile interval, i.e.,

$$K_B = \frac{\iint RSR_B(\lambda) \cdot L_{SD}(\lambda, \beta, \phi) \cdot h(\lambda) d\phi d\lambda}{\int RSR_B(\lambda) d\lambda}, \qquad (2)$$

is used to describe all manifested optical effects of the light from the SD registered by the observing band seen in this analysis. This formulation integrates away the dependence on declination angle to correctly match the summation approach of dn from the full-profile interval, and makes K_B a one-dimensional function of solar beta or azimuthal angle only. The construction of the K_B function is the critical step for extracting the final F-factor.

In principle, either solar beta angle or solar azimuthal angle is a legitimate choice as the second angle, in addition to solar declination angle, in the characterization function and analysis. Because solar beta angle β remains effectively constant within each orbit of the satellite and thus causes no ambiguity for the summation analysis, it is the more convenient choice adopted here. The azimuth angle varies non-trivially over the full-profile range, thus requiring a more complex description to characterize the effect. Therefore, this paper refers only to solar beta angle β for convenience of discussion.

The formalism for computing the full-profile F-factor is

$$f(B,D,M,G) = \frac{RVS_{B,SD} \cdot K_B}{\sum_{S,F} \sum_i c_i(B,D,M,G) \cdot dn(B,D,F,S)^i}, \qquad (3)$$

where B is band, D is detector, M is the side of the half-angle mirror (HAM) which is the scan mirror for the sensor, G is the gain status, RVS function accounts for the response-versus-scan angle (RVS) effect of HAM that depends on the operating wavelength of band B and at SD, K_B is the characterization function of the various optical effects as described in Eqn. (2), c_i are the pre-launch measured calibration coefficients with the index from 0 to 2, and dn is the digital number for the four specified setting. For SNPP VIIRS, the inclusion of RVS characterization is not strictly necessary since it is normalized to the SD angle of incidence (AOI) and therefore amounts only to a constant factor. The summation over scan S in the denominator operates over all scans in the full-profile interval, which effectively corresponds to integration over solar declination angel ϕ. This summation over the full-profile dn therefore removes the dependence on ϕ, and is the key step that significantly simplifies the ensuing characterization analysis. The remaining variation comes from dependence of the summed-dn on solar beta angle. The K_B function, as described above, holds the information of all optical effects external to the gain performance of the RSB, and serves as the adjustment to the summed-dn in leading to the RSB F-factor of the full-profile approach. In other words, the mission-long summed-dn data result is embedded with various optical effects, and K_B is the characterized function to be used to account for and remove the effects. The step-by-step procedure of this analysis to build the mission-long F-factor of the full-profile approach is based on Eqn. (3), and most fundamentally, the construction of the K_B function. The information of these effects is actually available within the mission-long summed-dn result, and a direct examination of its pattern yields the successful characterization of the K_B function. Because the effect should be yearly invariant, the analysis carried out as described below actually uses only a three-year period.

C. The Algorithm

The step-by-step extraction procedure leading to the full-profile F-factor first starts with constructing the mission-long result of the instrument data, dn, in the full-illumination interval of each on-orbit calibration event. The purported radiance as described in Eqn. (1), the amount of light from the SD reaching the RSB under the extended angular range, cannot directly be computed because C_{Geo} and τ_{SDS} are unknown. This analysis utilizes Eqn. (3) to build up a series of successively corrected intermediate F-factor functions to arrive at the new F-factor of the full-profile approach. The intermediate F-factor functions are not normalized, and are denoted in lower case letter such as *fn* for clarity.

The starting point of the intermediate F-factor functions is "F1-factor" function f_1, the denominator part of the F-factor in Eqn. (1) corresponding to the instrument signal, shown below as

$$f_1(B,D,M,G) = \frac{1}{\sum_{S,F} \sum_i c_i(B,D,M,G) \cdot dn(B,D,F,S)^i} \qquad (4)$$

for each calibration event, where the summation is over all dn within the interval of direct solar illumination, as exemplified in Fig. 4. As mentioned previously, the summation over scan S corresponds to integrating over solar declination angle. The result of the raw mission-long build-up of individual f_1 values from all calibration events for Band M1 Detector 1 high gain stage is shown in Fig. 5 (magenta curve) as the top curve among the three. It is useful to point out again that this function does not correspond to the radiance in Eqn. (1) or Eqn. (2) since effects such as SD degradation and the vignetting effect have not been removed, but is whereby miscellaneous effects are removed step-by-step. The f_1 function should not be dependent on solar declination angle but is expected to be dependent on solar beta angle.

The f_1 function can be readily corrected for the Earth-Sun distance leading to the "F2-factor" function f2 as

$$f_2(B,D,M,G) = \frac{f_1(B,D,M,G)}{d_{ES}^2} \qquad (5)$$

Figure 5 shows the corresponding Band M1 Detector 1 mission-long f_2 result (green curve), the middle curve of the three, corresponding to the summed instrument signals in the full profile per calibration event corrected for Earth-Sun distance. Expectedly, the distance-correction makes a small adjustment from the top curve, the f_1 result.

The f_2 function is further corrected for the degradation of SD, $h(\lambda_B)$ to arrive at the "F_3-factor" function f_3 as

$$f_3(B,D,M,G) = f_2(B,D,M,G) \cdot h(\lambda_B) \ . \qquad (6)$$

The SD degradation, or H-factor, is directly taken from the on-orbit characterization result described by Sun and Wang [9]. Figure 5 shows the corresponding mission-long f_3 result for Band M1 Detector 1 high gain stage (blue curve), the lowest curve among the three. It can be seen that the degradation of the SD is the dominant effect impacting the instrument signals over long-term, and its removal leads to a gentler trend (blue curve) at less than 5% over 5 years. A yearly modulation of about 10% peak-to-trough is seen to dominate the short-term pattern. The f_3 function is the long-term performance of the RSB detector embedded with various yearly-modulating optical effects. Within this modulation is the manifested effect of the extended BVP as previously discussed, and also of the partial illumination described by the C_{Geo} function. The empirical characterization of this yearly modulation wholly captures the combined effect without isolating each.

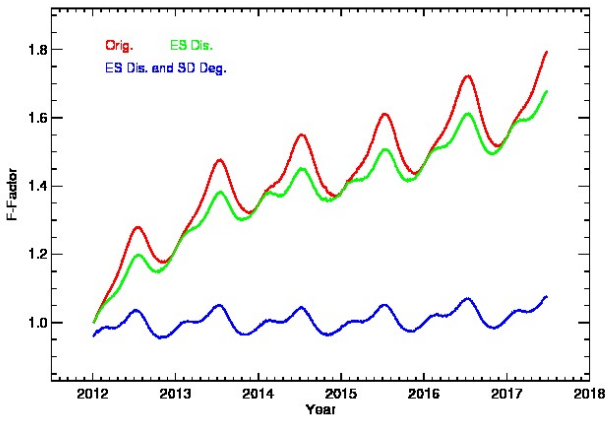

Fig. 5. SNPP VIIRS Band M1 Detector 1 high gain HAM side 1 F-Factor: Magenta curve is without any correction, f_1; Green curve is Sun-Earth distance effect corrected, f_2; Blue curve is Sun-Earth distance and SD degradation effects are corrected, f_3.

The extraction of the yearly modulation from f_3 is achieved through a straightforward fitting to a quadratic baseline function. For this purpose, the three-year period from the beginning of 2014 through the end of 2016, shown in Fig. 6, is selected for fitting. As to be shown and emphasized later, this three-year period has the most stable trend for all RSBs and is therefore selected for optimal fitting result. The observable yearly modulation in the f_3 function (red curve) is the manifestation of the combined optical effects such as from the BVP and the new characterization function C_{Geo}, thus in principle any integral number of years can be used to capture the invariant functions. As previously stated, an advantage of the empirical approach is that detailed knowledge of each function or contributing optical effect is unnecessary for as long as the combined manifested effects in the detector response can be fully characterized. The theoretical framework and the standard characterization procedure may not be fully accurate, and so the empirical characterization of the multi-year trend, both short- and long-term, provides the more rigorous and reliable result. The quadratic baseline fit (green curve) in Fig. 6 indicates preliminarily for the three-year period a change of about 2% for the performance of Band M1 Detector 1. The sole purpose of the baseline fit is to establish the underlying three-year F-factor trend upon which modulation can be characterized, and is not itself intended to characterize the long-term RSB performance. The modulation seen in Fig. 6 contains two contributions to be separately characterized, with the first being dependent on solar beta angle as to be described below. For clarity, the term "modulation" will be used to describe the general overall pattern to avoid confusion with the two individual contributions.

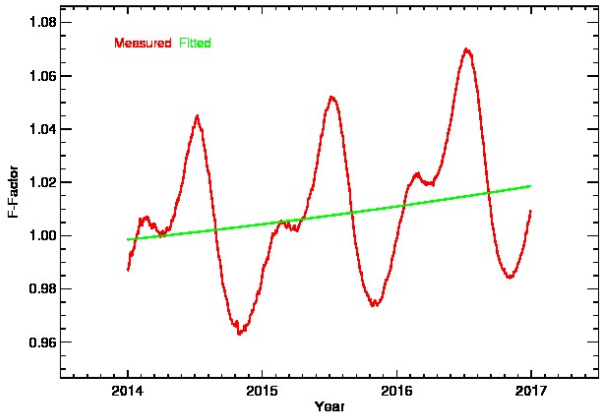

Fig. 6. SNPP VIIRS Band M1 Detector 1 high gain HAM side 1 F-factor: Magenta curve is Sun-Earth distance and SD degradation effects corrected F3-function, f_3; Green curve is quadratic form fitted to the measured data.

It can be seen in Fig. 6 that the three-year quadratic fit does not conform to the three-year trend of the f_3 function. For example, the fitted baseline is higher than the measured data at the beginning of 2015 but becomes lower at the beginning of 2016. That is, in addition to an underlying trend, the measured data show different shaping from year to year. This variation of the measured data against the baseline fit is correlated with the solar beta angle indeed as expected. Figure 7 shows the solar beta angle in the instrument coordinate frame of SNPP VIIRS over the six-year period since launch. The double-peak pattern, with the lowest points corresponding to near the end of each year, conforms to the pattern of f_3 shown in Figs. 5 and 6. The year-to-year change of the solar-beta is also consistent with the three-year trend in Fig. 6. It is readily obvious that the solar beta angle, which describes the orientation of the orbital plane of the satellite with respect to the solar position, directly impacts the illumination of the SD. The variation of the f_3 function against the quadratic baseline can be parameterized by

solar beta angle.

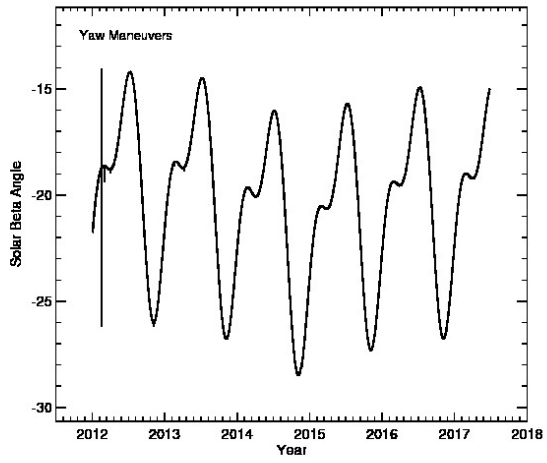

Fig. 7. SNPP VIIRS solar beta angle in instrument coordinate system.

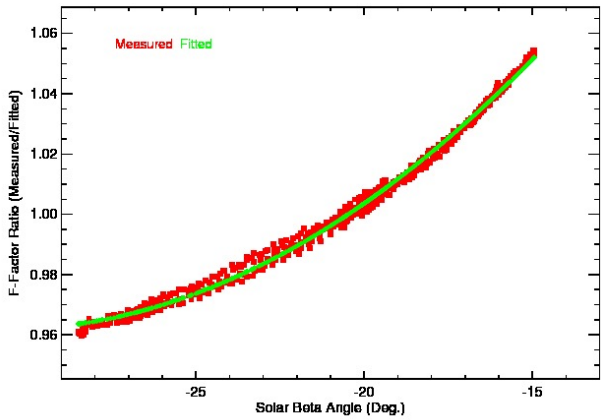

Fig. 8. Fitting residual of the Sun-Earth distance and SD degradation effects corrected F-factor, f_3, of SNPP Band M1 Detector 1 high gain HAM side 1, as shown in Fig. 6 versus solar beta angle, as shown in Fig. 7, in instrument coordinate, and the further fitting to a quadratic form in solar beta angle, $B(\beta)$. Symbols are the fitting residuals and solid curve is fitted quadratic form in solar beta angle, $B(\beta)$.

The characterization of the temporal variation associated with solar beta angle is carried out first by constructing a ratio of the f_3 function over the fitted baseline to remove the three-year baseline trend. The f_3-ratio, or the residual from the three-year fit, versus solar beta angle, is shown in Fig. 8 (red squares), and exhibits a clear non-linear relationship over its entire range. The general relationship between the f_3 residual and solar beta angle is very well described by the quadratic fit (green curve), $B(\beta)$, i.e.,

$$B(\beta) = c_0 + c_1 \cdot \beta + c_2 \cdot \beta^2 \qquad (7)$$

The quadratic fit to the f3 residual by Eqn. (7) is shown in Fig. 8 (green curve) and is seen to well trace the data over the entire range, apart from some minute deviation such as those in the middle of the range.

The "F_4-factor" function f_4 is constructed by removing the solar beta angle dependent function, $B(\beta)$, from the f_3 function as

$$f_4(B, D, M, G) = f_3(B, D, M, G) / B(\beta), \qquad (8)$$

thus the f4 function is the intermediate F-factor function corrected for Sun-Earth distance variation, SD degradation and also the impact of the solar angle.

It can be argued that, under the ideal scenario as also assumed by the standard methodology, the step-by-step extraction procedure reaching the f_4 function should be complete in capturing all considered effects including also the C_{Geo} function introduced in Eqn. (1) for compensating the effect of partial illumination. The crux of the argument is that direct solar illumination, full or partial, after correcting for SD degradation and d_{ES}, is strictly a function of the orbital plane with respect to the solar position, and this is described by the solar beta angle. Not only should the solar beta angle variation for the extended BVP captured by this characterization step, but so should the variation in C_{Geo} function. In other words, this characterization step should capture the combined beta angle dependent variation in BVP as well as in the C_{Geo} function provided that the C_{Geo} function fully describes partial illumination.

Although the variation in f_3 function over a 10% range appears to have been well captured by a parameterization of solar beta angle, as shown in Fig. 8, minute deviation of about 0.5% actually remains. Consequently, the removal of the $B(\beta)$ variation leading to the f_4 function still contains some small remnant of other optical or viewing-geometric effect that needs to be further characterized and removed. The remaining deviation between the f_3 residual and the solar beta angle parameterization is shown in Fig. 9, and is overlaid onto a one-year period. The pattern of the remaining residual (red squares) exhibits a two-peak annual cycle of about 0.6% peak-to-trough. It is clear by this result that an additional non-trivial variation exists beyond the solar beta angle characterization. The further best fit to this two-peak yearly pattern in the measured data is denoted by Δ_B (green curve).

This two-peak yearly oscillation is not a function of solar beta angle and is therefore not attributable to partial illumination. Furthermore, it is not associated with any other considerations known within the standard framework. The most likely explanation from all effects examined so far is the impact of the scattered light coming through the nadir-port, as shown by the weak signals in Figs. 3 and 4. These signals comes from light scattered of Earth's surface coming through the nadir port to illuminate the SD, which occurs during the entire daytime portion of the orbit as well as within a small range in the full profile of the direct solar illumination, primarily in the partial illumination interval as can be seen on the left side in Fig 4. This small leakage of light into the full-profile signal certainly will have an impact. A recent study has used this Earth scattered-light source, in the entire interval of the daytime portion of orbit where the Earth-scattered light signals are received, in another alternative calibration approach for RSB characterization and demonstrated a similar two-peak yearly pattern [17] associated with the Earth scattered light arising from the seasonal difference between the illumination of the two hemispheres. The low magnitude of the two-peak

yearly oscillation seen here at the 0.6% level is also consistent with the low level of the signals from the Earth-scattered light, exemplified in Fig. 3 to be only 0.6% of the full solar-illumination level. Thus, a more accurate description for the C_{Geo} function introduced in Eqn. (1) is to replace by $C = C_{Geo}*C_{Scat}$, with the C_{Scat} function describing the additional Earth scattered-light contribution characterized as Δ_B. This is the presumed origin of the Δ_B function. If the Earth-scattered light does not leak into the full-profile data, then $B(\beta)$ function alone would be sufficient without needing the extra characterization of Δ_B.

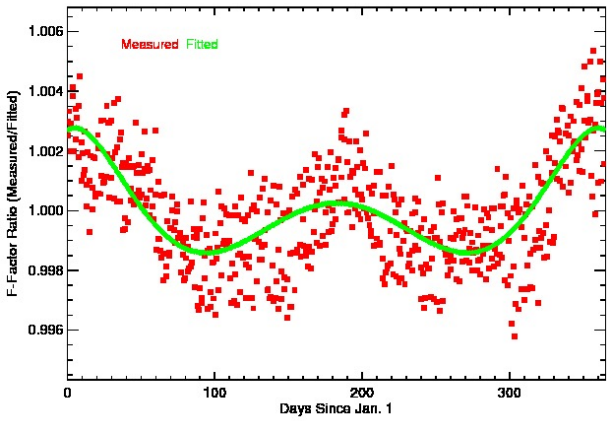

Fig. 9. Fitting residual of the quadratic form of the solar angle fitted to the fitting residuals of the quadratic form of the time as shown in Fig. 8, which cannot be described by solar beta angle but have a clear seasonal oscillation, and their further fitting to a smooth function of time with an annual oscillation, Δ_B. Symbols are the residuals and solid is fitted function of the time, Δ_B.

Finally, the "F_5-factor" function, f_5, is obtained via the removal of the two-peak yearly function Δ_B,

$$f_5(B,D,M,G) = f_4(B,D,M,G)/\Delta_B \quad . \qquad (9)$$

Figure 10 summarizes the three steps, f_3 (red), f_4 (green), and finally f_5 (blue) the mission-long F-factor of the full-profile approach, and furthermore the 16-day average (cyan). These curves are intentionally offset for clarity of illustration. As stated previously, the yearly pattern in f_3 contains two separate contributions, now characterized as $\Delta_B*B(\beta)$, and f_5 can be directly related to f_3 as $f_5 = f_3/(\Delta_B*B(\beta))$. The f_4 function as an intermediate step is constructed for better illustration of the detail in the overall modulation pattern.

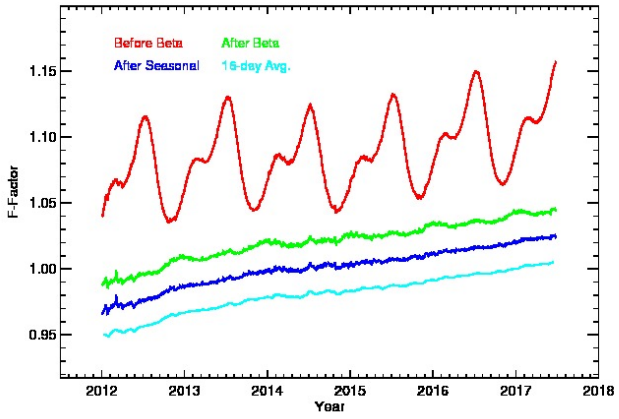

Fig. 10. SNPP VIIRS Band M1 Detector 1 high gain HAM side 1 F-Factor trends: Magenta curve is Sun-Earth distance and SD degradation effects corrected, f_3; Green curve is further solar angle dependence, $B(\beta)$, corrected, f_4; Blue curve is further annual oscillation, Δ_B, corrected, f_5; Cyan curve is the 16-day average. The curves are offset for purpose of illustration.

The K_B function as defined in Eqn. (2) is a theoretical description of the radiance connecting to the physical components and their associated effects. However, its characterization approach adopted here is akin to reverse engineering and empirically builds up a K_B function through the direct examination of the pattern within the data. The final form of the empirical characterization is

$$K_B = \frac{h_B}{B(\beta)\cdot\Delta_B\cdot d_{ES}^2}, \qquad (10)$$

which includes the additional Earth scattered-light contribution Δ_B. Eqn. (10) reveals the calibration calculation for each calibration event to amount to calculating a value from a well-defined function.

Finally, the full-profile F-factor is formally set to be the f_5 function as

$$f(B,D,M,G) = R\cdot f_5(B,D,M,G), \qquad (11)$$

where R is the remaining normalization to be referenced to an initial time at the early mission.

A succinct summary of the overall procedure is $f=R\cdot K_B\cdot f_1$, starting from the raw mission-long instrument data of the full profile of the direction solar illumination, f_1, and accordingly adjust the result by the K_B function. The K_B function is fully-characterized via Eqn. (10) without needing further re-analysis, and its application here or for any future studies of full-profile approach requires only the update of time, solar beta angle and also h_B, which has explicit time dependence but affecting only the overall constant, for computing the K_B at the time of interest to extract the corresponding F-factor.

The formalism has explicitly laid out the dependence on band, detector, HAM side and gain status, but numerous steps or functions require only a detector-averaged result. Figure 11 demonstrates the detector independence in the beta angle variation $B(\beta)$ for the mission-long result of band M1. It is seen that the mission-long patterns for all 16 detectors of band M1

are effectively indistinguishable. Expectedly, because solar angle is a geometric parameter of the instrument, any function of solar beta angle is necessarily the same for all detectors and the band, and this is true for BVP or C_{GEO}, or the combined effect. The description of the variational dependence for each band therefore requires only a single function for all detectors. In Fig. 11, it is also interesting to point out that the SNPP yaw maneuver in early 2012 appears in the solar beta angle plot as a sudden drop near the beginning of 2012.

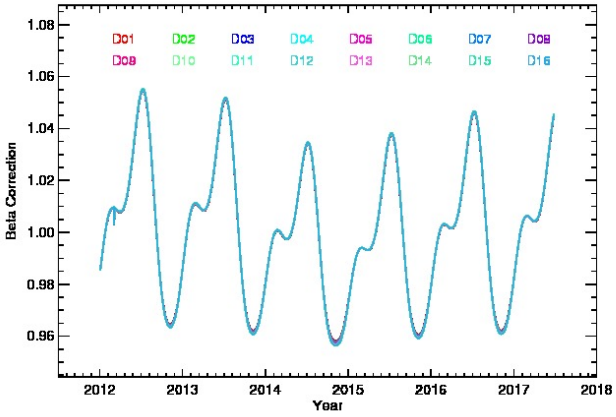

Fig. 11. Variation from solar beta angle, B(β), for all detectors of SNPP VIIRS Band M1.

Figure 12 shows the detector-averaged B(β) parameterization results for all RSBs. It is readily seen that the quadratic parameterizations show different behaviors among all RSBs. Specifically, the offsets, correspond to c_0 in Eqn. (7), are different as all parameterizations show relative offsets. The coefficients of the second term, corresponding to c_2, are also different due to distinctively different curvatures. Although the resulting variation slightly differs for each band or wavelength, all parameterizations remain close to one another and tightly conform to a quadratic form of solar beta angle. The differences among the parameterizations of different bands reflect the wavelength dependence in the extended BVP, described by Eqn. (1), specifically from the BRF of the SD. In principle, VF is a geometrical effect independent of band or wavelength, as has been fully discussed in Sun and Wang for SNPP VIIRS [15], as also the C_{Geo} function a geometric consideration. But the BRF of the SD is wavelength dependent, thus giving rise to the observed differences. The detector-independent but band-dependent result in the parametrization using solar beta angle is consistent with this understanding. In reality as already mentioned previously, the BRF is a two-dimensional function that requires more complex analysis; but the summation scheme here has simplified the dependence to only that of solar beta angle and enabled a much simpler analysis to characterize a one-dimensional variation in the mission-long data.

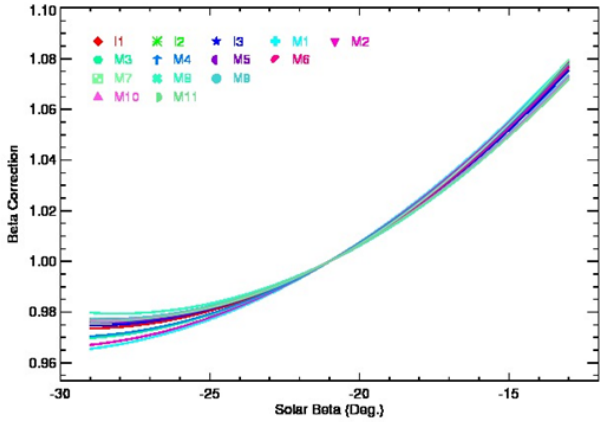

Fig. 12. Correction to F-factor by solar beta angle, $B(\beta)$, for all SNPP VIIRS RSBs.

The two-peak yearly pattern, Δ_B, for all detectors of band M1 reconstructed for the entire mission is shown in Fig. 13. The Δ_B function is expectedly independent of detector, showing only negligible differences between detectors at the 0.01% level. The detector-independence allows for a detector-averaged Δ_B to be used for analysis and for application. It is seen that the six-year pattern continues smoothly from one year to the next without discontinuity and mismatching slopes, demonstrating that the three-year fitting as exemplified in Fig. 9 correctly characterizes the function. The continuity and the matching slope conditions are not automatically guaranteed by any general fitting scheme, and a less careful fitting can possibly result in discontinuities and mismatching slopes.

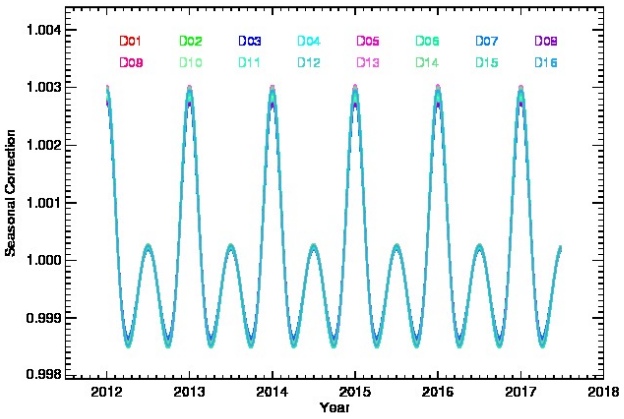

Fig. 13. Seasonal oscillation correction, Δ_B, for all detectors of SNPP VIIRS Band M1, showing negligible detector dependence.

The extracted Δ_B function for all 14 RSBs are shown in Fig. 14. Dependence on band or wavelength is apparent but with small differences at the level of 0.1% within the overall magnitude of oscillation at about 0.5%. This conforms to the expectation that the captured optical effects, being wavelength

dependent, behave with slight differences for different bands. All functions go through a similar double-peak yearly cycle that peaks in the Austral summer period when SNPP VIIRS makes more daytime observation of the southern hemisphere.

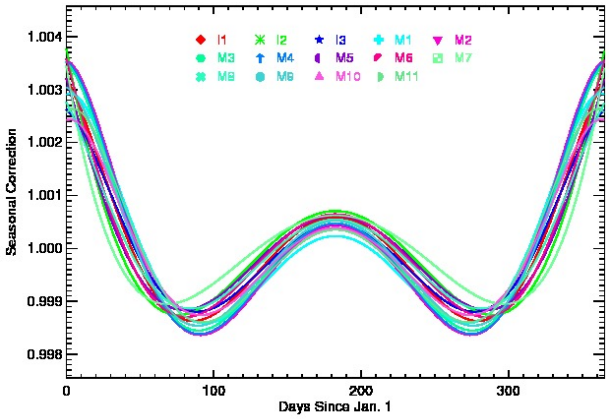

Fig. 14. Seasonal oscillation correction, Δ_B, for all SNPP VIIRS RSBs.

Table 1. Summary of the intermediate functions

f_1	Inverse of prelaunch radiance summation
f_2	The effect of the Earth-Sun distance removed
f_3	The effect of the SD degrdation corrected
f_4	The solar angle dependence removed
f_5	The minor impact due to the Earth scattered light removed

III. RESULTS AND DISCUSSION

The full-profile F-factor for each RSB is calculated for all detectors, gain statuses, and both HAM sides. The gain statuses for dual-gain bands are low-gain (LG) and high-gain (HG), and two sides of HAM are designated as HAM 1 and HAM 2. The full-profile F-factor for all Band M1 detectors are shown in Fig. 15 for HG HAM 1 (Fig. 15 corresponds to Fig. 6 in Ref [8]). The F-factor is normalized to the first point of the detector-averaged result. The result shows detector differences, similar trend of about 5% overall or 1% annually, no seasonal modulation, and stability at the 0.2% level. These results effectively duplicate that of the standard approach (Fig. 6, Ref [8]). The differences among detectors come from the pre-launch measured calibration coefficients ci, as in Eqn. (3). If the prelaunch coefficients have been accurately determined, then all F-factors will be seen to start at 1.0 and closely trace each other.

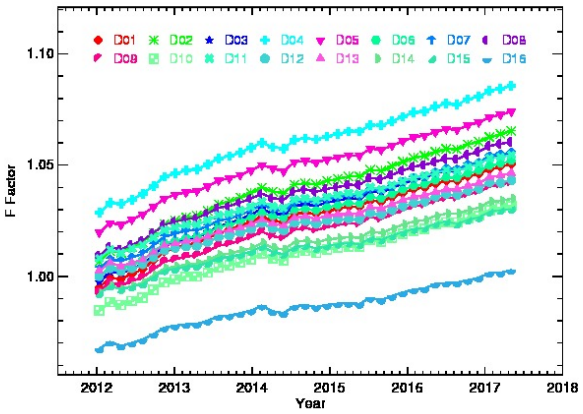

Fig. 15. Full-profile F-factor for SNPP VIIRS Band M1 high gain HAM side 1, normalized by the detector-averaged value of the first measurement.

The F-factor also depends on the HAM side and, for dual-gain bands, the gain status. The full-profile F-factor for the two HAM sides and gain statuses for Band M1 averaged over all detectors is shown in Fig. 16 (this figure corresponds to Fig. 9 in Ref [8]), expectedly displaying the differences between HAM sides and gain statuses. The F-Factor is normalized to the first point of the averaged HAM and gain status results, at 1.0 at the beginning of 2012. The four sets of F-factor trends similarly and maintains the same level of differences through out the mission, with two gain statuses consistently maintain a 2% difference and that the two HAM sides within each gain status differ by about 0.2%.

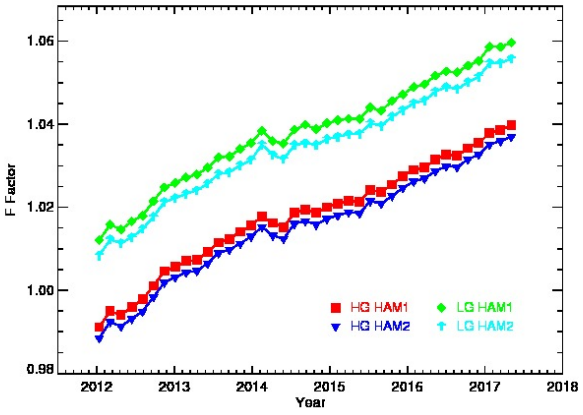

Fig. 16. SNPP VIIRS Band M1 detector-averaged F-Factor: Red squares represent high gain HAM side 1; Blue triangles represent low gain HAM side 1; Green diamonds represent high gain HAM side 2; Cyan arrows represent low gain HAM side 2.

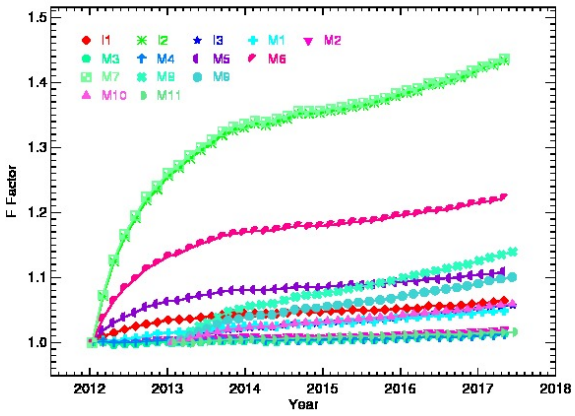

Fig. 17. Detector-averaged high gain HAM side 1 F-Factor for all SNPP VIIRS RSBs.

The mission-long full-profile detector-averaged F-factor for all RSBs, moderated bands M1−M11 and imagery bands I1−I3, are shown in Fig. 17. The shortwave infrared (SWIR) bands, M8−M11, are normalized to the beginning of 2013 [8] because SWIR bands were not stable before the tempearture of the SWIR focal plane was controlled. It can be seen that every RSB shows a clear and smooth mission-long F-factor for the full-profile approach. On the whole, the results agree with the stardand SD calibration result [8], which is to be shown later. Bands M7, M8 and I2 show the largest change as a group, at near 45% by near mid-2017, follow by M6 at about 22%. Most of the F-factor change occurs in the first two years of the mission, about 75% of the total change, and starting from 2014 and on the change becomes more gentle and almost linear while continues to trend upward.

The full-profile F-factor result is the direct extraction from the measured data, which are the dn in the full-profile of direct solar illumination, via the prescribed methodology without any smoothing, averaging or fitting scheme. The step-by-step empirical approach characterizes the long-term modulation unrelated to RSB performance, and removes it from the measured data. The analysis here is carefully constructed and carried out, and makes a clear separation between the F-factor trend from the external modulation. The prescribed fitting and characterization procedure is applied only to the modulation while leaving F-factor trend untouched. The procedure certainly relies on a very careful analysis to achieve the correct characterization, but once the baseline of the modulation is correctly established then the F-factor is readily extracted as a "residual against the fitted modulation baseline."

The use of the three-year period overlaid for a one-year fitting instead of the multi-year fitting of the entire mission to characterize the modulation is an important detail worthy of emphasizing. While F-factor is certainly the most important end result, a better understanding of these external effects is highly beneficial. It is first instructive to understand that the standard calibration methodology and operation is a carefully formulated framework allowing only a restricted and well-defined set of effects to be embedded within the long-term (trend) change of the band performance. These effects, independent of the band performance, can only be of short-term yearly pattern without contributing to long-term changes of the RSB performance. Example effects such as the vignetting effect of the attenuation screen are geometrical in nature necessarily following the geometrical variation as the satellite and the sensor move through its yearly cycle around the Sun, resulting in a repeated yearly pattern that remains identical from one year to the next. The analysis here also reveals a small additional yearly variation attributed to the impact from the Earth scattered-light coming through the nadir port, and is presumed to be a manifestation of the yearly variation of the global property of the Earth reflectance due to changing seasons, the yearly variation in the viewing geometry of the sensor, and other seasonal effects. The yearly variation is also presumed to be multi-year invariant over the time scale of SNPP mission, although it is entirely possible for the conditions to Earth to undergo detectable changes over time scales of decades. The Sun et al. [17] study using the Earth scattered light has already provided a clear result in support of the invariance of the global yearly reflectance property of Earth during the SNPP mission to date. The result shown in this analysis demonstrates similarly. The yearly invariance of the overall modulation in the mission-long data therefore permits the use of a limited time period for characterization of the yearly modulation.

Overall, the invariant $B(\beta)$ and Δ_B functions only need to be characterized once and can be used as is for the entire mission and for future studies of SNPP VIIRS as previously mentioned. Since they are mainly geometric effects, although the BRF of the SD remains weakly dependent on wavelength, the two functions derive from SNPP VIIRS may be also applicable for the follow-on VIIRS instruments. It will be interesting to study the corresponding invariant functions in future VIIRS.

The gain change of the RSBs has significantly flattened in the later years in comparison to the earlier mission, and therefore the use of the three-year period from 2014 to the end of the 2016 is most stable for an accurate fitting of the underlying trend as previously stated. The inclusion of the earlier data in fact results in worse accuracy and is also entirely unnecessary. The eventual stability of the new F-factor at the level of 0.1% demonstrates the correctness of the approach and the physical understanding underneath it. While using the entire mission for multi-year fitting can possibly achieve a similar successful characterization of the modulation, it fundamentally handles the effect from one year to the next as independent and thus does not help to confirm the yearly invariance of the modulation. The one-year overlay fitting approach using a selected three-year period, on the other hand, necessarily relies on the invariance assumption for the result to be applicable mission-long, and will fail if invariance is otherwise false. The successful F-factor result showing smoothness at the 0.1% stability level with no modulation is indicative of the correctness of the invariance condition and the fitting procedure that fully capture the modulation.

IV. SD DEGRADATION NON-UNIFORMITY AND GENERAL DISCUSSION

Results from the previous section fully demonstrate the success of the full-profile approach as an independent methodology using a very different approach, but also valuable is its result displaying the known RSB calibration discrepancy [12-14] arising from the SDDNU effect, which refers to the anisotropic degradation of the SD reflectance with respect to both the incident and outgoing angles that is contrary to a key assumption of the standard calibration methodology. Earlier studies of the standard SD-based calibration and other approaches, such as lunar [18-21] and Earth target-based calibration [10,11], have already revealed for many years the existence of some worsening error coming from within the standard RSB calibration methodology. A dedicated examination of the mission-long data in the "sweet spot" for SNPP VIIRS, Terra and Aqua MODIS [14] have demonstrated the evolving angular dependence with respect to the range of the incident angle of the "sweet spot", thus proving the SDDNU effect. The standard on-orbit RSB calibration methodology [22] for VIIRS as well as for MODIS [6,7] assumes the SDSM-measured H-factor, characterizing the on-orbit degradation of the SD reflectance in the outgoing angle from the SD toward the SDSM with respect to the normal SD, to be a valid substitute for SD degradation at other outgoing angles. The standard approach thus assumes the SD degradation to be the same at all incident or outgoing angles when reality proves this assumption false. The performance characterization of RSBs in SNPP VIIRS requires SD degradation in the direction from the SD to the RTA that directs light to the RSB. Because the angle to the RTA is at a different outgoing angle from the SDSM-measured H-factor, the applied H-factor is therefore incompatible for characterizing the RSB due to the SDDNU effect and consequently calibration error ensues. In fact, the calibration bias in the standard approach increases with time as the SDDNU effect worsens [14], and the error is particularly pronounced for the four shortest wavelength bands, M1−M4 [12,13].

The full-profile F-factor is built from data in the entire interval of direct solar illumination of the SD, with its angular range of the incident light from the Sun to the SD to be wider than that of the standard approach, which is a small "sweet spot" sub-interval in the full illumination. Due to this difference, the full-profile F-factor is expected to exhibit a different result from the standard F-factor because of the SDDNU effect. Figure 18 shows the extracted full-profile F-factor (symbols) in an overlay with the standard F-factor (solid curves) for bands M1−M7 through mid-2017. The overall change for M5, M6 and M7 is very significant at close to 10%, 30% and 65%, respectively, and yet the agreement between the full-profile and the standard result for these three bands is within 0.1% difference. The agreement is expected since the full-profile F-factor is extracted as is from the measured data and should reflect the true gain change for the bands. However, M1 F-factor, at about 5% change over the mission, exhibits some discrepancy between the full-profile (red diamonds) and the standard results (red line), revealing the anticipated impact of the SDDNU effect that most significantly affects band M1.

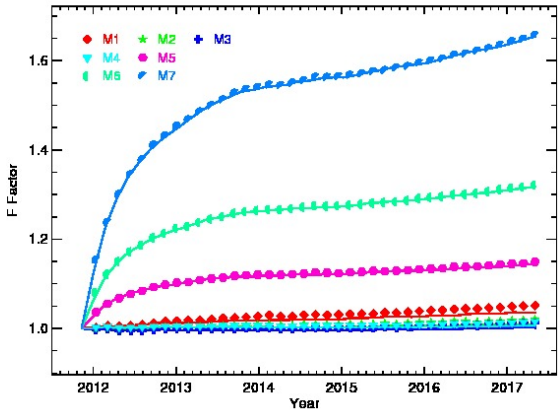

Fig. 18. Detector-averaged high gain HAM side 1 F-Factor for all SNPP VIIRS RSBs: Symbols represent full profile F-factor; Solid lines represent standard F-factor computed with data in the sweet spot.

Figure 19 shows a comparison of the full-profile F-factor (symbols) with the standard F-factor (solid curves) for bands M1−M4 over a smaller 5% range for a clearer exposition of the impact of the SDDNU effect in these four shorter wavelength bands. The overall discrepancy between the full-profile and the standard F-factor for bands M1−M4 reaches an estimated difference of 1.5%, 1%, 1% and 0.7%, respectively, after five years. The overall band-dependence of the result, such as band M1 showing the greatest discrepancy, and the level of disagreement on the order of 1% is consistent with previous findings [12,13]. The difference between the full-profile and the standard result due to the SDDNU effect for these four bands is likely to widen further, and the discrepancy for band M1 is estimated to breach 2% by the end of 2019. In addition, the full-profile results confirm the additional complication in bands M3 and M4 [8] also visible in the standard result. The M4 F-factor breaks the pattern of the apparent band or wavelength dependence and becomes higher than the M3 F-factor, which signals the existence of another effect in addition to the SDDNU effect.

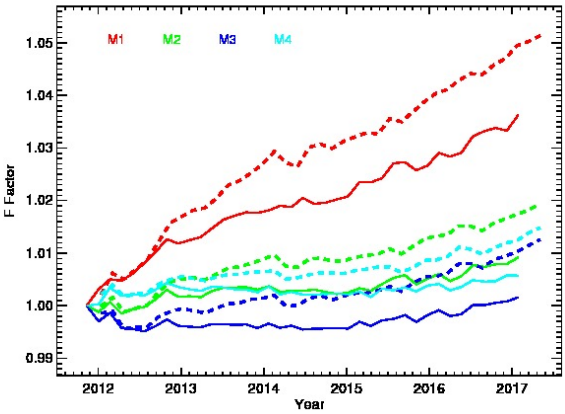

Fig. 19. Detector-averaged high gain HAM side 1 F-Factor for SNPP VIIRS bands M1-M4: Dotted lines represents full-profile F-factor; Solid lines represent standard F-factor computed with data in the sweet spot.

Figure 19 adds in the result of the lunar-based calibration (symbols) for comparison. Between the full-profile and the lunar-based results, the bands M1 (red diamonds) and M2 (green stars) F-factors agree reasonably on the order of 0.3%. However, their M3 results diverge up to 0.5% and the band M4 results differ up to 1%. This finding further supports the existence of some additional effect impacting bands M3 and M4 [12-14]. The dedicated study of the SDDNU effect [14] has previously quantified the SDDNU impact to be small in bands M3 and M4, therefore the discrepancy with the lunar-calibration result as shown in both the standard result [12-13] and here the full-profile result points to an additional effect whose impact on M3 and M4 is much as 1% over five years. Nevertheless, it is interesting to see that the full-profile F-factors are closer to the lunar result than the standard result, but discrepancy still persists.

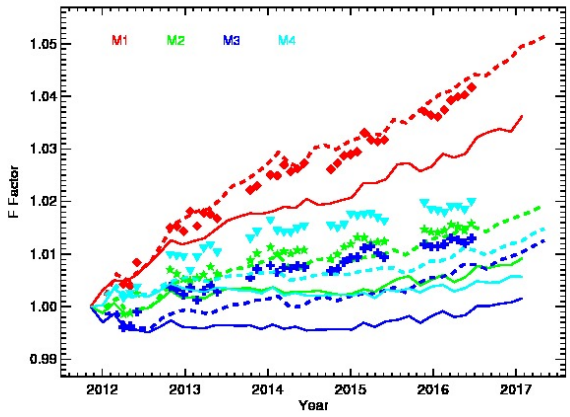

Fig. 20. Detector-averaged high gain HAM side 1 F-Factor for all SNPP VIIRS bands M1-M4: Symbols, lunar calibration; Dotted lines, full profile; Solid lines, currently standard approach with data in the sweet spot.

The angular range of the full profile of the direct solar illumination extends but entirely covers the sweet spot, and therefore the full-profile F-factor is made discrepant from the standard F-factor by the contribution from illumination intervals external to the sweet spot. The full-profile result thus unambiguously demonstrates the impact of the SDDNU effect strictly because of the difference in the outgoing angles from of the illumination from the SD to the RTA. Interestingly as similarly mentioned above, the full-profile F-factors are in much closer agreement to the lunar-based "hybrid-method" F-factor [12,13] constructed to correct the RSB calibration error in of SNPP VIIRS. While there is otherwise no known connection beyond a coincidence, nevertheless if the full-profile F-factors have been used, the calibration error and the discrepant performance in science products [23,24] may have proceeded unnoticed, and investigations into the SDDNU effect may have yielded a less decisive conclusion. In all cases, it is worthy to note that the full-profile result remains discrepant with the lunar result, demonstrating the impact of the SDDNU effect on any SD-based calibration approach.

Sun et al. [17] have also recently investigated another variant of the RSB calibration in SNPP VIIRS using light scattered off Earth's surface coming through the nadir port as the source of illumination for the SD. In the Earth scattered-light approach, the incident angle of the light source is from the nadir port to the SD, different from the incident direction in the standard approach that is from the SD port to the SD. The F-factor from the Earth scattered-light approach also shows good long-term agreement with the standard F-factor for bands M5−M8, but discrepant results for bands M1−M4. The Earth scattered-light approach thus demonstrates the impact of the SDDNU effect due to the different incident angles of light impinging on the SD. With the full-profile approach herein demonstrating the impact of the SDDNU due to different outgoing angles, the combined studies into the SD-based RSB calibration for SNPP VIIRS have successfully shown the impact of the non-trivial behavior in SD degradation on RSB calibration for both the incoming and outdoing angles, that the BRDF of the SD changes functionally in all of its angular dependence as SD degrades on orbit. The dedicated study into the SDDNU effect for SNPP VIIRS and the twin MODIS [14] has examined the dependence of the effect with respect to the outgoing angle but appeals to the principle of optical reciprocity in order to draw further conclusion on the dependence of the effect on the incident angle. The full-profile result presented here completes the direct proof the difference in the F-factor result due to a different angular range of the incident light.

The standard, Earth-scattered light and full-profile approaches essentially amount to showing the different SD-based calibration approaches as a matter of choice for the first step in RSB calibration. Each approach generates its own unique set of F-factors, however smooth or robust, different from the others. But because of the non-trivial angular dependence of the reflectance property of SD degradation, and perhaps also of other effects not yet addressed, mitigation such as the "hybrid-method" is necessary for each SD-based approach as the second step. Overall, this study further clarifies the shortcoming within the standard on-orbit calibration strategy as well as any SD-based alternatives due to the non-ideal property of the BRDF of the SD and strengthens the understanding for the long-term mitigation for any version of the SD-based calibration. NOAA-20 VIIRS and other future VIIRS definitively will need to contend with this troublesome issue.

The analysis procedure itself does not try to explicitly reconstruct any components in Eqns. (1) or (2), and is also not concerned with the accuracy of the description. The modulation in the mission-long data is instead examined and empirically characterized without any explicit study of the effect, as would be needed to derive the extended BVP. The overall pattern of the data is a straightforward combination of the RSB performance embedded with various effects manifested as yearly modulation, and therefore the removal of the modulating pattern readily leads to the F-factor. The added clarity into the behavior of the mission-long data, and how various components impart its effects into the result, is an added value of this investigation. This is a viable and general analysis approach to characterize all miscellaneous effect whole and use it to extract the F-factor, and should be applicable to other similar new-generational sensors.

V. Conclusion

A new variant using the full-profile of the direct solar illumination of the SD for the on-orbit RSB calibration of SNPP VIIRS is demonstrated to be robust. The step-by-step extraction procedure using the data from the full profile of direct solar illumination successfully characterizes the external seasonal effects, and isolates the F-factor that characterizes the on-orbit gain change of the bands. Without needing to use any pre-derived two-dimensional BRFs of the SD or the VFs of the solar attenuation screen, this work has potentially important implication for RSB calibration and satellite yaw operation. A three-year period is shown to suffice for the characterization of the yearly invariant functions accounting for effects of solar-beta angle and Earth-scattered light. The full-profile F-factor result is stable on the level of 0.1% to 0.2%. The full-profile and the standard F-factor agrees remarkably well for bands M5−M7, but show diverging result for bands M1−M4 up to 1.5% due to the impact of the SDDNU effect. The finding continues to highlight the impact and importance of the SDDNU effect as well as the additional effect for bands M3 and M4 that needs to be examined. The study advances a new consideration for the on-orbit calibration analysis of RSBs and demonstrates a set of empirical invariant functions that is more straightforward and reliable for use with the on-orbit calibration. But any SD-based calibration analysis remains only as the first step with it results to be further corrected for the SDDNU effect via a completely separately analysis.

Acknowledgment

This work was supported by the Joint Polar Satellite System (JPSS) funding. The views, opinions, and findings contained in this paper are those of the authors and should not be construed as an official NOAA or U.S. Government position, policy, or decision.

References

[1] W. L. Barnes and V. V. Salomonson, “MODIS: A global imaging spectroradiometer for the Earth Observing System,” Crit. Rev. Opt. Sci. Technol. CR47, 285-307 (1993).

[2] B. Guenther, W. Barnes, E. Knight, J. Barker, J. Harnden, R. Weber, M. Roberto, G. Godden, H. Montgomery, and P. Abel, “MODIS Calibration: A brief review of the strategy for the at-launch calibration approach”, J of Atmospheric and Oceanic Technology 12, 274-285 (1996).

[3] C. Cao, F. Deluccia, X. Xiong, R. Wolfe, F. Weng, “Early on-orbit performance of the Visible Infrared Imaging Radiometer Suite (VIIRS) onboard the Suomi National Polar-orbiting Partnership (S-NPP) satellite,” IEEE Trans. Geosci. Remote Sens. 52, 1142–1156 (2014).

[4] C. Donlon, B. Berruti, A. Buongiorno, M.-H. Ferreira, P. Féménias, J. Frerick, P. Goryl, U. Klein, H. Laur, C. Mavrocordatos, J. Nieke, H. Rebhan, B. Seitz, J. Stroede, R. Sciarra, “The global monitoring for environment and security (GMES) sentinel-3 mission, ” Remote Sensing of Environment 120, 37-57 (2012).

[5] C. J. Bruegge, A. E. Stiegman, R. A. Rainen and A. W. Springsteen, “use of Spectralon as a diffuse reflectance standard for in-flight calibration of earth-orbiting sensors,” Opt. Eng. 32, 805-814 (1993).

[6] X. Xiong, J. Sun, W. Barnes, V. Salomonson, J. Esposito, H. Erives, and B. Guenther, "Multiyear on-orbit calibration and performance of Terra MODIS reflective solar bands", IEEE Trans. Geosci. Remote Sens. 45, 879-889 (2007).

[7] X. Xiong, J. Sun, X. Xie, W. L. Barnes, and V. V. Salomonson, “On-orbit calibration and performance of Aqua MODIS reflective solar bands,” IEEE Trans. Geosci. Remote Sens. 48, 535–545 (2010).

[8] J. Sun and M. Wang, “On-orbit calibration of the Visible Infrared Imaging Radiometer Suite reflective solar bands and its challenges using a solar diffuser,” Appl. Opt. 54, 7210-7223 (2015).

[9] J. Sun and M. Wang, "Visible Infrared imaging radiometer suite solar diffuser calibration and its challenges using solar diffuser stability monitor", Appl. Opt. 53, 8571-8584 (2014).

[10] J. Sun, X. Xiong, A. Angal, H. Chen, A. Wu, and X. Geng, “Time dependent response versus scan angle for MODIS reflective solar bands,” IEEE Trans. Geosci. Remote Sens., 52, 3159-3174 (2014).

[11] J. Sun, A. Angal, X. Xiong, H. Chen, X. Geng, A. Wu, T. Choi, and M. Chu, "MODIS RSB calibration improvements in Collection 6", Proc. SPIE 8528, 85280N (2012).

[12] J. Sun and M. Wang, “Radiometric calibration of the visible infrared imaging radiometer suite reflective solar bands with robust characterizations and hybrid calibration coefficients,” Appl. Opt., 54, 9331-9342 (2015).

[13] J. Sun and M. Wang, "VIIRS reflective solar bands calibration progress and its impact on ocean color products", Remote Sens. 8, 194 (2016).

[14] J. Sun, M. Chu and M. Wang, “Degradation nonuniformity in the solar diffuser bidirectional reflectance distribution function,” Appl. Opt. 55, 6001-6016 (2016).

[15] J. Sun and M. Wang, “On-orbit characterization of the VIIRS solar diffuser and solar diffuser screen," Appl. Opt. 54, 236-252 (2015).

[16] J. McIntire, D. Moyer, B. Efremova, H. Oudrari, X. Xiaoxiong, “On-orbit characterization of S-NPP VIIRS transmission functions”, IEEE Trans. Geosci. Remote Sens. 53, 2354-2365 (2015).

[17] J. Sun, M. Chu, and M. Wang, “Visible Infrared Imaging Radiometer Suite reflective solar bands on-orbit calibration using solar diffuser illuminated by scattered light through the nadir port”, Appl. Opt., 57, 1273-1283 (2018).

[18] T. C. Stone and H. H. Kieffer, "Use of the Moon to support on-orbit sensor calibration for climate change measurements," Proc. SPIE 6296, 62960Y-1-9 (2006).

[19] J. Sun, X. Xiong, W. L. Barnes, and B. Guenther, “MODIS reflective solar bands on-orbit lunar calibration”, IEEE Trans. Geosci. Remote Sens. 43, 2383-2393 (2007).

[20] J. Sun, X. Xiong, and J. Butler, “NPP VIIRS on-orbit calibration and characterization using the Moon,” Proc. SPIE 8510, 85101I (2012).

[21] X. Xiong, J. Sun, J. Fulbright, Z. Wang, and J. Butler, “Lunar calibration and performance for S-NPP VIIRS reflective solar bands”, IEEE Trans. Geosci. Remote Sensing. 54, 1052-1061 (2016).

[22] N. Baker, “Joint Polar Satellite System (JPSS) VIIRS radiometric calibration algorithm theoretical basis document (ATBD),” Goddard Space Flight Center, Greenbelt, Maryland, NASA, May 15, 2013.

[23] Wang, M., X. Liu, L. Jiang, S. Son, J. Sun, W. Shi, L. Tan, P. Naik, K. Mikelsons, X. Wang, and V. Lance, "VIIRS ocean color research and applications", Proc. IGARSS '15, pp.2911-2914 (2015).

[24] Wang, M., L. Jiang, X. Liu, S. Son, J. Sun, W. Shi, L. Tan, K. Mikelsons, X. Wang, and V. Lance, "VIIRS ocean color products: A progress update", Proc. IGARSS '16, pp.5848-5851 (2016).